

Discovery of Adamantane Carboxamides as Ebola Virus Cell Entry and Glycoprotein Inhibitors

Michael B. Plewe, Nadezda V. Sokolova, Vidyasagar Reddy Gantla, Eric R. Brown, Shibani Naik, Alexandra Fetsko, Donald D. Lorimer, David M. Dranow, Hayden Smutney, Jameson Bullen, Rana Sidhu, Arshil Master, Junru Wang, E. Adam Kallel, Lihong Zhang, Birte Kalveram, Alexander N. Freiberg, Greg Henkel, and Ken McCormack*



Cite This: <https://dx.doi.org/10.1021/acsmedchemlett.0c00025>



Read Online

ACCESS |



Metrics & More



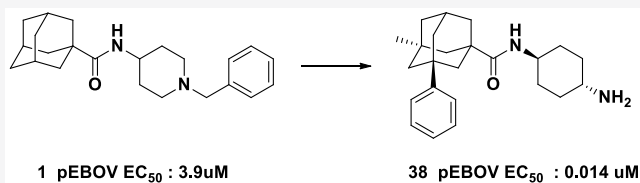
Article Recommendations



Supporting Information

ABSTRACT: We identified and explored the structure–activity–relationship (SAR) of an adamantane carboxamide chemical series of Ebola virus (EBOV) inhibitors. Selected analogs exhibited half-maximal inhibitory concentrations (EC_{50} values) of ~ 10 – 15 nM in vesicular stomatitis virus (VSV) pseudotyped EBOV (pEBOV) infectivity assays, low hundred nanomolar EC_{50} activity against wild type EBOV, aqueous solubility >20 mg/mL, and attractive metabolic stability in human and nonhuman liver microsomes. X-ray cocrystallographic characterizations of a lead compound with the EBOV glycoprotein (GP) established the EBOV GP as a target for direct compound inhibitory activity and further provided relevant structural models that may assist in identifying optimized therapeutic candidates.

KEYWORDS: Ebola virus, glycoprotein, cell entry, adamantane carboxamide



EBOV is a single stranded RNA virus associated with severe hemorrhagic fever exhibiting $>50\%$ lethality in humans.^{1,2} Symptoms typically manifest with generalized fever, sore throat, and muscular pain whereupon vomiting, diarrhea, and both internal and external bleeding may follow; transmission of EBOV is spread through contact with these bodily fluids. The development of EBOV vaccines as well as intravenous (i.v.) administered monoclonal antibody and small molecule therapeutics, many of which focus on the EBOV glycoprotein (GP) and/or viral cell entry, has recently drawn intensive interest; the testing and utilization of these treatments was accelerated in response to major EBOV outbreaks in West Africa and the Democratic Republic of the Congo (DRC).^{3–5} However, despite the availability of effective vaccine and i.v. administered therapeutics, the DRC Kivu outbreak continued to escalate and spread geographically from August 2018 through August 2019 at which time the number of new cases began to stabilize and subsequently decrease.⁶ Thus, a significant need remains in some resource settings for the development of more convenient and readily distributable therapeutics including oral small molecule treatment options.

EBOV GP, the sole protein expressed on the EBOV envelope membrane surface, is responsible for host cell attachment, endosomal entry, and membrane fusion. The EBOV GP is trimeric, with each monomer cleaved by furin into two polypeptides, GP1 and GP2. The entry of EBOV into host cells is initiated by the interaction of sites on GP1 subunits with one or more receptors exposed on the host cell external membrane surface, upon which the virus is

internalized into endosomes primarily via micropinocytosis.^{3–5,7} Within acidified endosomes glycosylated GP1 is cleaved of a “mucin-domain” into a smaller form by the pH-dependent Cathepsin L and B proteases, priming it for interactions with the Niemann Pick C1 (NPC1) protein, a secondary intracellular receptor in endosomal/lysosomal membranes. NPC1 binding, in combination with other events, triggers GP conformational rearrangements including GP2-mediated fusion of viral and intracellular organelle membranes thereby releasing EBOV genetic material into the cell for further replication.^{7–9}

A number of antibody-based EBOV therapeutics bind to GP blocking early cell entry steps while small molecule EBOV cell entry inhibitors have primarily been reported to block later steps in viral entry/fusion by interacting with a number of intracellular mammalian host proteins regulating EBOV transport, processing, and membrane fusion or, alternatively, directly with the viral GP protein.^{3–5,8–13} We utilized a biosafety level 2 (BSL2) nonreplicative vesicular stomatitis virus (VSV) pseudotyped virus system in which VSV viral particles express a luciferase reporter gene (in place of the VSV GP

Received: January 15, 2020

Accepted: April 21, 2020



gene) while the EBOV GP is supplied *in trans*, to rapidly screen a chemical library and characterize compound hits.¹⁴ Utilizing this approach we screened a collection of small molecules representing ~72,000 compounds in Vero cells at 5 μ M to identify compounds inhibiting 50% of the luciferase signal generated by infection with pEBOV without similar activity against control pVSV infected cells.

We report the discovery and initial SAR of an adamantane carboxamide chemical series of pEBOV inhibitor compounds identified from our library screen as hit compound **1**, which exhibited >50% activity at 5 μ M against pEBOV but not pVSV. **1** was then subjected to concentration–response experiments and found to exhibit an EC_{50} of ~3.9 μ M. We subsequently obtained commercially available analogs of **1**, and identified **2**, which exhibited a ~10-fold greater pEBOV potency (Figure 1). As **2** differed from **1** only by the addition of a phenyl group

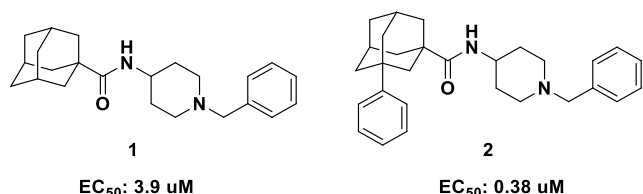
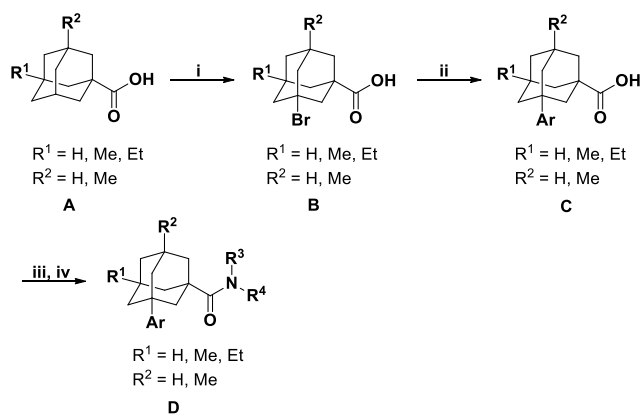


Figure 1. Screening hit compound **1** and its phenyl analog **2** with indicated pEBOV EC_{50} values.

to the adamantane core, we were interested in further SAR exploration of phenyl adamantane carboxamides. We subsequently generated analogs with modifications of the phenyl adamantane core as well as the amine portion as illustrated in Scheme 1 (see Supporting Information for synthesis details and analytical data).

Scheme 1. Synthesis of Aryl Adamantane Carboxamides^a



^aReagents and conditions: (i) Br_2 , Fe, 0 $^{\circ}C$ for 30 min, then rt, 8 h; (ii) $AlCl_3$, Ar–H, reflux, 6 h; (iii) R^3R^4NH , EDC hydrochloride, HOAt, DIEA, DCM, rt, 12 h; (iv) TFA, DCM, rt, 2 h.

A number of amine groups were thus initially explored as shown by compounds **3**–**8** in Table 1. Comparing the homologous series of compounds **2**, **3**, and **5** illustrated a link between modifications of the terminal amine and improved potency. In addition, comparison of pEBOV activities of the tetrahydroisoquinoline compound **8** (a commercially available compound) vs the 4-aminopiperidine of compound **5** also suggested that the basicity and hydrogen

bonding ability of terminal amine play an important role in determining binding affinity.

We subsequently explored the addition of several substituents at the para-position of the phenyl group. Unfortunately, both polar and nonpolar groups were found to decrease compound potency as shown for compounds **9**–**13**. Nonpolar substituents such as Cl resulted in decreased activity (**11** vs **5**) while more polar groups including OH caused a more significant loss of activity (**10** vs **5**) indicating that para substitutions on phenyl groups are not well tolerated.

Given the synthetic challenges associated with the generation of similar ortho- and meta-phenyl substituted analogs and further exploration of the phenyl group, we next focused on modifications of the amide position, replacement of the adamantane core with noradamantane, introduction of a spacer between the adamantyl moiety and amide functionality, and amide group replacements that are illustrated by compounds **14**–**19** in Table 2 (see Supporting Information, Schemes S1–S5 for the synthesis of intermediates and final compounds). Transposition of the amide group to an adjacent secondary carbon, giving compound **14**, decreased potency approximately 3-fold from the analogous tertiary carbon amide **5**, whereas noradamantyl **15**, acetamide **16**, reverse amide **17**, urea **18**, and diamine **19** analogs all exhibited even greater decreases in pEBOV potency.

Since each of the different amide group replacements (compounds **16**–**19**) decreased pEBOV potency, we next explored the introduction of additional substituents into the adamantane core (Supporting Information) and generated novel phenyl adamantane carboxamides bearing alkyl groups at the bridgehead positions. The addition of two methyl groups into the adamantane core of compound **20** (Core D-1, Table 3) resulted in a ~4-fold decrease in pEBOV potency compared to compound **5**, whereas in contrast, the addition of a single methyl group (Core D-2, Table 3) improved potency about ~2-fold as observed in pEBOV activity comparisons of compounds **21** vs **5**. We subsequently generated additional analogs of Core D-2 by coupling 3-methyl-5-phenyladamantane-1-carboxylic acid with a variety of different mono Boc-protected diamines, followed by cleavage of the Boc-group under acidic conditions (Table 3, Scheme 1, steps iii and iv). Both cyclic and bicyclic amines of different ring sizes containing an exocyclic or endocyclic nitrogen, as well as acyclic amines have been investigated. Although substituted aminopiperidines (compounds **22** and **23**) have similar potency to compound **21**, other amines (compounds **24**–**27** and **29**) exhibited decreased activity. Other novel amines (compounds **28**, **30**, **31**, and **33**), particularly *trans*-cyclohexyldiamine (compound **33**) showed promising activity while *cis*-cyclohexyldiamine (compound **32**) is less active. These trends further suggested the importance of the protonated amine group to conform within a specified geometry in association with its target protein, given the observed improvement with addition of a single methyl substituent at the adamantane bridgehead position protein. Given the observed improvement with the addition of a single methyl substituent at the adamantane bridgehead position (Core D-2), we also explored replacement of the methyl group with the larger and more lipophilic ethyl group (Core D-3, Table 3), which further increased potency (compare **34** vs **21** and **35** vs **33**) to provide compounds with $EC_{50}s \leq 20$ nM. Upon the identification of analogs with improved compound potencies, we subsequently assessed the SAR of prioritized compounds

Table 1. SAR of 3-Aryladamantane Carboxamides Exploring Various Amines and Aryl Groups

| # | Compound | pEBOV* EC ₅₀ (μM) | # | Compound | pEBOV* EC ₅₀ (μM) | # | Compound | pEBOV* EC ₅₀ (μM) |
|---|----------|---------------------------------|---|----------|---------------------------------|----|----------|---------------------------------|
| 2 | | 0.38 | 6 | | 0.12 | 10 | | 1.7 |
| 3 | | 0.16 | 7 | | 0.26 | 11 | | 0.19 |
| 4 | | 0.28 | 8 | | 2.3 | 12 | | 0.31 |
| 5 | | 0.072 | 9 | | 0.38 | 13 | | >3.0 |

*Data are average of three independent experiments, standard deviation (s.d.) ≤ 20%.

for potential metabolic liabilities. Compounds exhibiting EC₅₀ values of ~ ≤150 nM were evaluated for *in vitro* human liver microsome (HLM) metabolic stability. Core D-2 compounds **21**, **31**, and **33** exhibited pEBOV EC₅₀s < 50 nM and HLM stability >75% at 1 h while core D-3 compounds **34** and **35** exhibited EC₅₀s ≤ 20 nM and slightly lower HLM stabilities of ~70%. These analogs were used as the basis of further exploration and the 4-aminopiperidine (**21**), *trans*-4-(aminomethyl)cyclohexylamine (**31**), and *trans*-cyclohexyldiamines (**33** and **35**) appeared to provide particularly attractive lead candidates. Kinetic aqueous solubilities (Supporting Information) were also assessed for all compounds described in this report and each exhibited a kinetic aqueous solubility >100 μM at pH 6.4 and 7.5 except compound **27**, which exhibited a solubility of ~61 μM.

Because the adamantane nucleus forms a perfect tetrahedron, adamantanes with four unique substituents at the bridgehead positions are chiral. Hence, the addition of the methyl and ethyl groups to the phenyladamantane carboxamide core (Cores D-2 and D-3) generates chiral compounds with the chiral center residing in the center of the adamantane. In light of this, we next generated the (1*S*,3*R*,5*R*,7*S*)- (abbreviated as *S*) and (1*R*,3*S*,5*S*,7*R*)- (abbreviated as *R*) enantiomers of the prioritized racemic analogs **21**, **31**, **33**, and **35** (Supporting Information). As shown in Table 4, the *S* enantiomers are eutomers exhibiting a greater potency than the *R* enantiomers. The potency differences between the *S* and *R* enantiomers of the ethyl (**42** vs **43**) and methyl derivatives (**38** vs **39**) were ~30 and 10-fold, respectively while the rank order SAR of pEBOV activity for racemic and *S* enantiomeric compounds was similar.

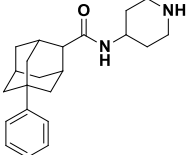
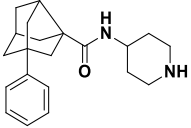
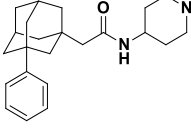
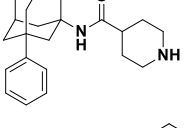
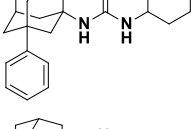
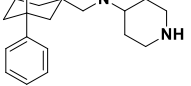
In addition to pEBOV potency (EC₅₀ values) the Hill slopes and activity curves of the compounds are all roughly equivalent

as observed in the concentration–response relationships of the *S* enantiomeric compounds plotted in Figure 2. Of note, the Hill slopes are all substantially greater than 1 (Table 4) indicating a positive cooperativity underlying the inhibitory activity of each of the compounds.

In order to confirm that compound inhibitory activities observed in the pEBOV assay format translate to activity against replicative pathogenic EBOV, the prioritized *S* enantiomers were characterized in plaque or viral yield reduction (VYR) assays (Supporting Information) as shown in Table 4. Comparison of the EBOV EC₉₀ (from the VYR assay) values vs the half-maximal cellular cytotoxicity or CC₅₀ provides SI₉₀ therapeutic selectivity indices ([CC₅₀]/[EC₉₀]) for compounds **36**, **38**, and **40** of 34, 77, and 40, respectively. Compound **42** was only run in the plaque assay and exhibited an SI₅₀ value ([CC₅₀]/[EC₅₀]) of 221. These data confirm the antiviral activity of the compounds against replicative EBOV with potencies that translate in similar rank order to that found against pEBOV. There is however, an offset in EBOV vs pEBOV potencies, whereby EC₅₀s against infectious EBOV correlate more closely with EC₉₀s against the pseudotyped virus pEBOV. Nonetheless, the discovery and potency optimization of our prioritized analogs from our initial screening hit compound **1** vs **38**, **40**, and **42** (pEBOV EC₅₀ improvement from ~3.9 μM to ~10 nM) further validates the use of BSL2 pseudotyped viral systems for the discovery of novel inhibitors of highly pathogenic BSL4 viruses.

For additional SAR comparison and compound prioritization we further characterized the solubility of the *S*-enantiomers **36**, **38**, **40**, and **42** and found them all to exhibit >20 mg/mL aqueous solubility at pH 7.4. To provide additional assessments for advancement into one or more *in vivo* animal model studies, we subsequently characterized **36**,

Table 2. SAR Exploration of Functional Group Spacers

| # | Compound | pEBOV* EC ₅₀ (uM) |
|----|---|---------------------------------|
| 14 |  | 0.18 |
| 15 |  | 0.33 |
| 16 |  | 0.49 |
| 17 |  | >1.0 |
| 18 |  | >1.0 |
| 19 |  | 0.47 |

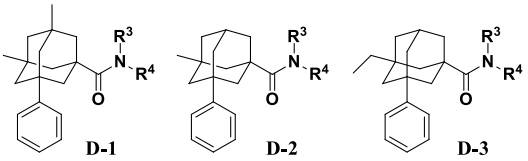
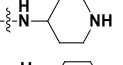
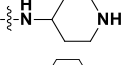
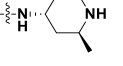
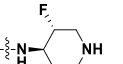
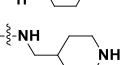
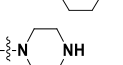
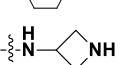
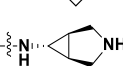
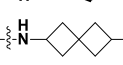
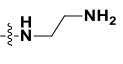
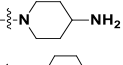
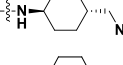
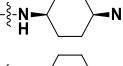
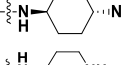
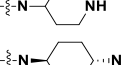
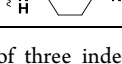
*Data are averages of three independent experiments, s.d. \leq 20%.

38, 40, and 42 in multispecies liver microsome (MLM) metabolic stability assays including human and the potential efficacy and/or toxicology model species mouse, guinea pig, rat, cynomolgus monkey, and dog. While each of the S analogs exhibited suitable HLM metabolic stability, compounds 36 and 38 provided the most favorable MLM metabolic stability profile. Further *in vitro* and *in vivo* ADMET characterizations of these prioritized analogs will be assessed to identify lead candidates and suitable species for *in vivo* efficacy and toxicology studies.

Herein, we have detailed the discovery and initial SAR of a novel adamantane carboxamide chemical series of EBOV inhibitors. Previous reports identifying inhibitors of EBOV cell entry have provided a number of targets that include a variety of potential mammalian host proteins regulating intracellular EBOV processing, transport, and membrane fusion, as well as the EBOV GP itself, which has been identified as the target for several FDA-approved drugs.^{3–5,8–13,15,16} Interestingly, the adamantane chemical series identified here is structurally related to an adamantane dipeptide piperazine EBOV inhibitor chemical series found to associate with the mammalian host protein and intracellular GP receptor NPC1.⁸ Thus, it was initially expected that NPC1 might also represent the target for our adamantane carboxamide EBOV inhibitor chemical series.

To identify the target and potential mechanism of action of our inhibitor compounds, we determined X-ray cocrystallo-

Table 3. Adamantane Carboxamides Core SAR

|  | | | | |
|--|------|---|---------------------------------|-------|
| # | Core | R ³ R ⁴ NH | pEBOV* EC ₅₀ (uM) | HLM** |
| 20 | D-1 |  | 0.32 | - |
| 21 | D-2 |  | 0.043 | 75 |
| 22 | D-2 |  | 0.046 | 75 |
| 23 | D-2 |  | 0.033 | 60 |
| 24 | D-2 |  | 0.42 | - |
| 25 | D-2 |  | 0.13 | 100 |
| 26 | D-2 |  | 0.28 | - |
| 27 | D-2 |  | 0.12 | - |
| 28 | D-2 |  | 0.040 | 79 |
| 29 | D-2 |  | 0.25 | - |
| 30 | D-2 |  | 0.051 | 81 |
| 31 | D-2 |  | 0.030 | 75 |
| 32 | D-2 |  | 0.11 | 87 |
| 33 | D-2 |  | 0.031 | 92 |
| 34 | D-3 |  | 0.020 | 69 |
| 35 | D-3 |  | 0.010 | 71 |

*Data are averages of three independent experiments, s.d. \leq 20%.

**Percent remaining at 60 min. HLM: human liver microsomes.

graphic structures of the EBOV GP protein with compound 38. In Figure 3 we provide structural representations generated through crystallization of the apo protein with subsequent soaking of the crystals with 38 similar to that previously described (Supporting Information).¹³ As mentioned above, the functional EBOV GP complex is comprised of a trimer of GP1-GP2 dimers. In panels A–D (Figure 3) the GP binding pocket, located at the interface of each GP1-GP2 dimer, and specific amino acid interactions underlying association with 38 are depicted. The binding pocket is characterized by hydrophobic residues defining a central hydrophobic cavity to accommodate the adamantane core and phenyl group of 38 (analog with a phenyl group showed increased potency of ~10-fold) through lipophilic GP1 residues VAL66, LEU184, and LEU186 as well as GP2 residues LEU515, TYR517,

Table 4. Ebola Virus Inhibitory Activity, Cytotoxicity, and Liver Microsomal Stability of Enantiomeric Adamantane Carboxamides

[illegible]

*. Data are average of three independent experiments, standard deviation $\leq 20\%$. ** $n = 3$, standard deviation $< 20\%$. *** Percent remaining after 60 min, H: Human, M: Mouse, G: Guinea Pig, R: Rat, MK: Monkey, D: Dog.

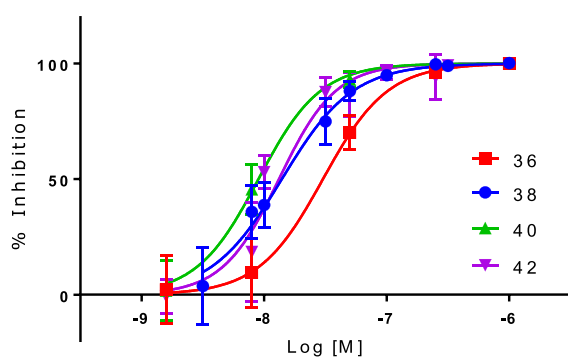


Figure 2. Concentration–response curves of prioritized S-enantiomers against pEBOV \pm s.d. ($n = 3$); the cooperative Hill slopes ranged from 1.4 to 1.7 (Table 4).

MET548, and LEU558, while the carbonyl of the amide forms an important hydrogen bond with ARG64.

In binding to the EBOV GP compound **38** displaces a GP1 polypeptide loop that is normally bound within this pocket in the apo conformation. This GP1 polypeptide loop, previously defined as comprising residues 192–194 (the “DFF lid”), was previously found to be displaced by toremifene and a number of other small molecules.^{13,15–17} The association of **38** with the EBOV GP parallels that of other compounds although as represented in Figure 3 (panel B) GP1 polypeptide residues 193–195 (residues FFS) appear to bind within the apo pocket and overlap with bound compound **38** while D192 appears to lie outside of a shared binding pocket. However the boundaries of the apo polypeptide loop or “lid” may be defined, the binding of a GP inhibitor to this site displaces the GP1 loop and alters GP conformation thereby preventing fusion between the viral and endosomal membranes. Such ligand induced

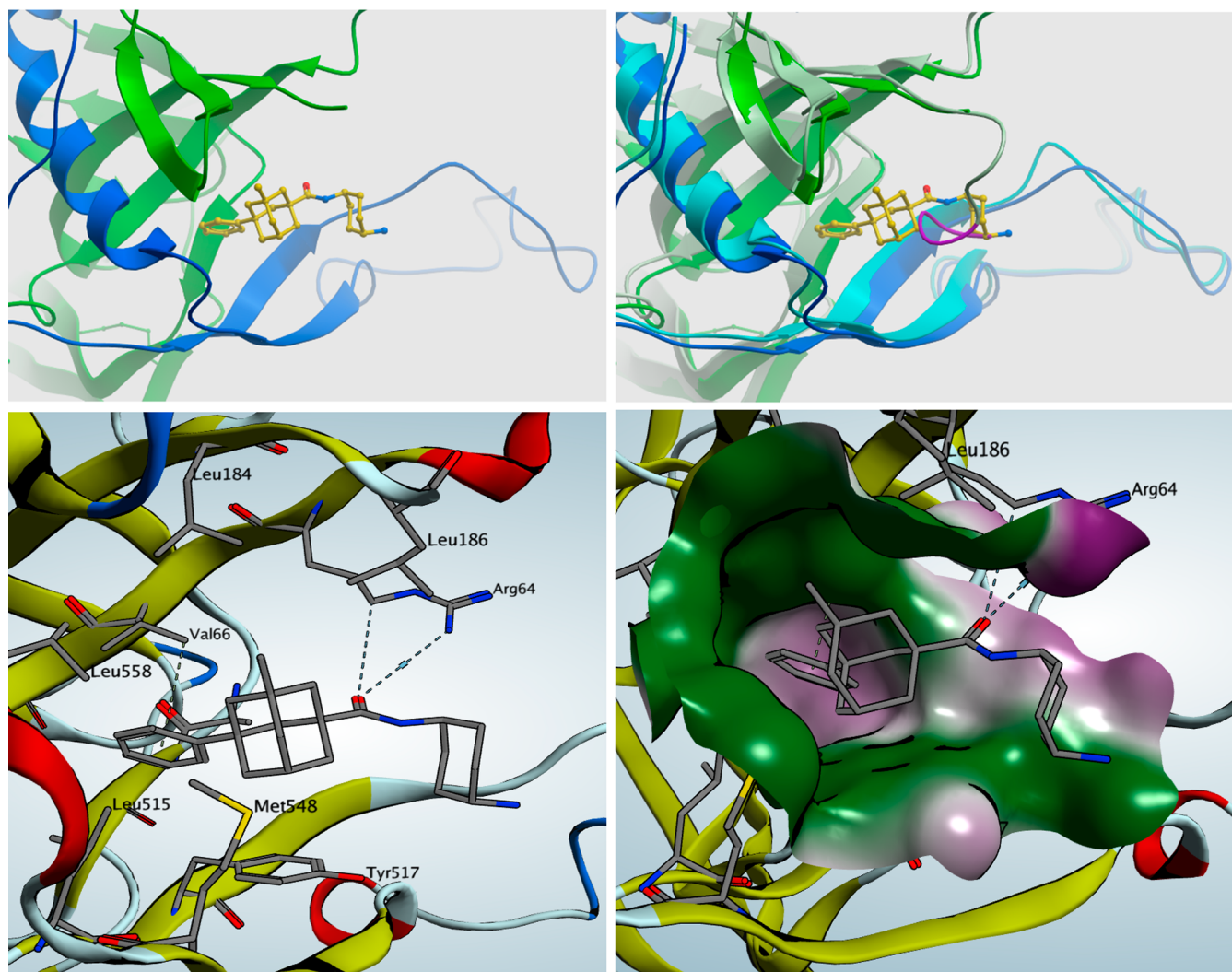


Figure 3. X-ray cocrystallographic structures of compound **38** bound to the EBOV GP. (Panel A) (top left) Compound **38** (yellow) binding pocket located at the GP1 (dark green)–GP2 (dark blue) dimer interface. (Panel B) (top right) Overlay of the apo GP1 (light green) and GP2 (light blue) and **38**-bound GP1 (dark green) and GP2 (dark blue) protein structures. Residues 193–195 (amino acids FFS) in the apo conformation GP1 polypeptide are highlighted (purple) and exhibit overlap with compound **38** in a shared binding pocket. (Panel C) (bottom left) GP binding pocket for **38** and residues determining important ligand–protein interactions including lipophilic GP1 residues VAL66, LEU184, and LEU186 and GP2 residues LEU515, TYR517, MET548, and LEU558. (Panel D) (bottom right) Lipophilic (purple) and hydrophilic (green) molecular surfaces of GP showing the central cavity accommodating the adamantane core, lipophilic phenyl pocket, and amide/cyclohexylamine association sites with ARG64.

conformational changes may inhibit GP function through compound-specific mechanisms including premature release of GP2 and/or deficient GP processing, both of which could disrupt engagement with its receptor NPC1.^{13,15–17} Regardless of the potential for any compound-specific mechanisms for these inhibitors, toremifene exhibits an EC_{50} of ~ 80 nM in our pEBOV assays while another recently identified EBOV GP inhibitor (**118a**) has a reported pEBOV EC_{50} of ~ 50 nM in comparison to the adamantane carboxamide GP inhibitors described here, of which some exhibit pEBOV EC_{50} s in the range of ~ 10 – 14 nM.¹⁷

Given that the EBOV GP is composed of a trimer of GP1–GP2 dimers with three potential inhibitor binding sites, along with the positive cooperativity observed in the Hill slopes of the prioritized compound inhibition curves (Table 4 and Figure 2), it appears likely that the adamantane carboxamide inhibitor molecules act allosterically whereby the binding of one molecule to an initial GP1–GP2 dimer enhances the

binding of additional inhibitor molecules to other GP1–GP2 dimers within the same GP1–GP2 trimeric complex in order to fully abrogate EBOV GP function and viral replication. GP inhibitors exhibiting steeper Hill slopes would thereby be expected to provide superior antiviral activity.

In summary, we have identified a novel adamantane carboxamide chemical series and prioritized analogs exhibiting potent activity against pEBOV and replicative EBOV, which directly bind to and inhibit the EBOV GP. Selected lead compounds also exhibit attractive aqueous (HCl salt) solubility >20 mg/mL and multispecies *in vitro* liver microsome metabolic stability to provide candidates for the further development of novel small molecule therapeutics. The determination of a binding site and relevant structural models may also facilitate structure-based drug design of the adamantane carboxamide chemical series to provide the identification of improved therapeutic candidates.

■ ASSOCIATED CONTENT

SI Supporting Information

The Supporting Information is available free of charge at <https://pubs.acs.org/doi/10.1021/acsmmedchemlett.0c00025>.

Experimental procedures and synthetic schemes, analytical data, pseudotyped virus generation and assay, infectious wild type Ebola virus plaque assay, virus yield reduction (VYR) assay, liver microsome metabolic stability assay, solubility and cytotoxicity assays; Ebola GP protein expression, purification, crystallization, and structure determination. The atomic coordinates and structure factors have been deposited with the RCSB Protein Data Bank under accession code 6NAE. (PDF)

■ AUTHOR INFORMATION

Corresponding Author

Ken McCormack — Arisan Therapeutics, San Diego, California 92121, United States; orcid.org/0000-0003-1181-9137; Phone: (858) 766-0495; Email: kenm@arisanthera.com

Authors

Michael B. Plewe — Arisan Therapeutics, San Diego, California 92121, United States

Nadezda V. Sokolova — Arisan Therapeutics, San Diego, California 92121, United States

Vidyasagar Reddy Gantla — Arisan Therapeutics, San Diego, California 92121, United States

Eric R. Brown — Arisan Therapeutics, San Diego, California 92121, United States

Shibani Naik — Arisan Therapeutics, San Diego, California 92121, United States

Alexandra Fetsko — Arisan Therapeutics, San Diego, California 92121, United States

Donald D. Lorimer — Seattle Structural Genomics Center for Infectious Disease (SSGCID), Seattle, Washington 98105, United States; UCB Pharma, Bainbridge Island, Washington 98110, United States

David M. Dranow — Seattle Structural Genomics Center for Infectious Disease (SSGCID), Seattle, Washington 98105, United States; UCB Pharma, Bainbridge Island, Washington 98110, United States

Hayden Smutney — Seattle Structural Genomics Center for Infectious Disease (SSGCID), Seattle, Washington 98105, United States; UCB Pharma, Bedford, Massachusetts 01730, United States

Jameson Bullen — Seattle Structural Genomics Center for Infectious Disease (SSGCID), Seattle, Washington 98105, United States; UCB Pharma, Bainbridge Island, Washington 98110, United States

Rana Sidhu — Seattle Structural Genomics Center for Infectious Disease (SSGCID), Seattle, Washington 98105, United States; UCB Pharma, Bedford, Massachusetts 01730, United States

Arshil Master — Seattle Structural Genomics Center for Infectious Disease (SSGCID), Seattle, Washington 98105, United States; UCB Pharma, Bedford, Massachusetts 01730, United States

Junru Wang — Seattle Structural Genomics Center for Infectious Disease (SSGCID), Seattle, Washington 98105, United States; UCB Pharma, Bedford, Massachusetts 01730, United States

E. Adam Kallel — Victrix, San Diego, California 92128, United States

Lihong Zhang — Department of Pathology, The University of Texas Medical Branch, Galveston, Texas 77555, United States
Birte Kalveram — Department of Pathology, The University of Texas Medical Branch, Galveston, Texas 77555, United States
Alexander N. Freiberg — Department of Pathology and Center for Biodefense and Emerging Infectious Diseases, The University of Texas Medical Branch, Galveston, Texas 77555, United States

Greg Henkel — Arisan Therapeutics, San Diego, California 92121, United States

Complete contact information is available at: <https://pubs.acs.org/10.1021/acsmmedchemlett.0c00025>

Funding

This work was funded in whole or in part with Federal funds from the National Institute of Allergy and Infectious Diseases, National Institutes of Health, Department of Health and Human Services, under SIBR grants R43AI118207 and R43AI138878 and Contract #HHSN272201700059C.

Notes

The authors declare no competing financial interest.

■ ACKNOWLEDGMENTS

Arisan Therapeutics has utilized the nonclinical and preclinical services program offered by the National Institute of Allergy and Infectious Diseases.

■ ABBREVIATIONS

EBOV, Ebola virus;; VSV, vesicular stomatitis virus; GP, glycoprotein; pEBOV, pseudotyped VSV expressing the EBOV GP; HLM, human liver microsomes; MLM, multispecies liver microsomes; i.v., intravenous; SAR, structure–activity-relationships; VYR, viral yield reduction; BSL4, biosafety level 4; NPC1, Niemann Pick C1 protein; ADMET, absorption, distribution, metabolism, excretion, and toxicity; DCM, dichloromethane; DMF, *N,N*-dimethylformamide; TFA, trifluoroacetic acid; DIEA, *N,N*-diisopropylethylamine; EDC, 1-ethyl-3-(3-(dimethylamino)propyl)carbodiimide; RT, room temperature; Me, methyl; Et, ethyl; HOAt, 1-hydroxy-7-azabenzotriazole; Boc, *tert*-butoxycarbonyl.

■ REFERENCES

- (1) Rojas, M.; Monsalve, D. M.; Pacheco, Y.; Acosta-Ampudia, Y.; Ramirez-Santana, C.; Ansari, A. A.; Gershwin, M. E.; Anaya, J. M. Ebola Virus Disease: An Emerging and Re-Emerging Viral Threat. *J. Autoimmun.* **2020**, 106, 102375. No. October.
- (2) Burk, R.; Bollinger, L.; Johnson, J. C.; Wada, J.; Radoshitzky, S. R.; Palacios, G.; Bavari, S.; Jahrling, P. B.; Kuhn, J. H. Neglected Filoviruses. *FEMS Microbiol. Rev.* **2016**, 40 (4), 494–519.
- (3) Hoenen, T.; Groseth, A.; Feldmann, H. Therapeutic Strategies to Target the Ebola Virus Life Cycle. *Nat. Rev. Microbiol.* **2019**, 17 (10), 593–606.
- (4) Furuyama, W.; Marzi, A. Ebola Virus: Pathogenesis and Countermeasure Development. *Annu. Rev. Virol.* **2019**, 6 (1), 435–458.
- (5) Edwards, M. R.; Basler, C. F. Current Status of Small Molecule Drug Development for Ebola Virus and Other Filoviruses. *Curr. Opin. Virol.* **2019**, 35, 42–56.
- (6) Oppenheim, B.; Lidow, N.; Ayscue, P.; Saylor, K.; Mbala, P.; Kumakamba, C.; Kleinman, M. Knowledge and Beliefs about Ebola Virus in a Conflict-Affected Area: Early Evidence from the North Kivu Outbreak. *J. Glob. Health* **2019**, 9 (2), 020311.

- (7) Rhein, B. A.; Maury, W. J. Ebola Virus Entry into Host Cells: Identifying Therapeutic Strategies. *Curr. Clin. Microbiol. Reports* **2015**, *2* (3), 115–124.
- (8) Côté, M.; Misasi, J.; Ren, T.; Bruchez, A.; Lee, K.; Filone, C. M.; Hensley, L.; Li, Q.; Ory, D.; Chandran, K.; et al. Small Molecule Inhibitors Reveal Niemann–Pick C1 Is Essential for Ebola Virus Infection. *Nature* **2011**, *477* (7364), 344–348.
- (9) Fénéant, L.; Szymańska-de Wijs, K. M.; Nelson, E. A.; White, J. M. An Exploration of Conditions Proposed to Trigger the Ebola Virus Glycoprotein for Fusion. *PLoS One* **2019**, *14* (7), 1–20.
- (10) Flint, M.; Chatterjee, P.; Lin, D. L.; McMullan, L. K.; Shrivastava-Ranjan, P.; Bergeron, E.; Lo, M. K.; Welch, S. R.; Nichol, S. T.; Tai, A. W.; et al. A Genome-Wide CRISPR Screen Identifies N-Acetylglucosamine-1-Phosphate Transferase as a Potential Antiviral Target for Ebola Virus. *Nat. Commun.* **2019**, *10* (1), 285.
- (11) Penny, C. J.; Vassileva, K.; Jha, A.; Yuan, Y.; Chee, X.; Yates, E.; Mazzon, M.; Kilpatrick, B. S.; Muallem, S.; Marsh, M.; et al. Mining of Ebola Virus Entry Inhibitors Identifies Approved Drugs as Two-Pore Channel Pore Blockers. *Biochim. Biophys. Acta, Mol. Cell Res.* **2019**, *1866* (7), 1151–1161.
- (12) Salata, C.; Calistri, A.; Alvisi, G.; Celestino, M.; Parolin, C.; Palù, G. Ebola Virus Entry: From Molecular Characterization to Drug Discovery. *Viruses* **2019**, *11* (3), 274.
- (13) Zhao, Y.; Ren, J.; Harlos, K.; Jones, D. M.; Zeltina, A.; Bowden, T. A.; Padilla-Parra, S.; Fry, E. E.; Stuart, D. I. Toremfene Interacts with and Destabilizes the Ebola Virus Glycoprotein. *Nature* **2016**, *535* (7610), 169–172.
- (14) Garbutt, M.; Liebscher, R.; Wahl-Jensen, V.; Jones, S.; Möller, P.; Wagner, R.; Volchkov, V.; Klenk, H.-D.; Feldmann, H.; Ströher, U. Properties of Replication-Competent Vesicular Stomatitis Virus Vectors Expressing Glycoproteins of Filoviruses and Arenaviruses. *J. Virol.* **2004**, *78* (10), 5458 LP–5465.
- (15) Ren, J.; Zhao, Y.; Fry, E. E.; Stuart, D. I. Target Identification and Mode of Action of Four Chemically Divergent Drugs against Ebolavirus Infection. *J. Med. Chem.* **2018**, *61* (3), 724–733.
- (16) Zhao, Y.; Ren, J.; Fry, E. E.; Xiao, J.; Townsend, A. R.; Stuart, D. I. Structures of Ebola Virus Glycoprotein Complexes with Tricyclic Antidepressant and Antipsychotic Drugs. *J. Med. Chem.* **2018**, *61* (11), 4938–4945.
- (17) Shaikh, F.; Zhao, Y.; Alvarez, L.; Iliopoulou, M.; Lohans, C.; Schofield, C. J.; Padilla-Parra, S.; Siu, S. W. I.; Fry, E. E.; Ren, J.; et al. Structure-Based in Silico Screening Identifies a Potent Ebolavirus Inhibitor from a Traditional Chinese Medicine Library. *J. Med. Chem.* **2019**, *62* (6), 2928–2937.